Heat Flow Model of the Continuous Slab Casting Mold, Interface, and Shell

Brian G. Thomas, Bryant Ho, and Guowei Li

University of Illinois at Urbana-Champaign
Dept. of Mechanical and Industrial Engineering
1206 W. Green Street,
Urbana, IL 61801
Phone: 217-333-1176

ABSTRACT

This paper describes the formulation and application of a comprehensive heat flow model of the continuous casting process for steel slabs, focusing on phenomena in the mold region. The model includes a 1-D transient finite-difference calculation of heat conduction within the solidifying steel shell coupled with 2-D steady-state heat conduction within the mold wall. The model features a detailed treatment of the interfacial gap between the shell and mold, including mass and momentum balances on the solid and liquid powder layers. The model predicts the solidified shell thickness down the mold, temperature in the mold and shell, thickness of the resolidified and liquid powder layers, heat flux distribution down the mold, mold water temperature rise, ideal taper of the mold walls, and other related phenomena. The important effect of non-uniform distribution of superheat is incorporated using the results from previous 3-D turbulent fluid flow calculations within the liquid cavity. The effects of oscillation mark shape and mold curvature on heat transfer and the powder layers are also included. The FORTRAN program, CON1D, has a user-friendly interface and executes in less than a minute on a personal computer. Calibration of the model with experimental measurements on an operating slab caster is presented along with several example applications.

1. INTRODUCTION

Heat transfer in the continuous casting mold is governed by many complex phenomena. Fig. 1 shows a schematic of some of these. Liquid metal flows into the mold cavity through a submerged entry nozzle, and is directed by the angle and geometry of the nozzle ports.[1] The direction of the steel jet controls turbulent fluid flow in liquid cavity, which affects delivery of superheat to solid / liquid interface of the growing shell. In addition, this flow influences meniscus heat transfer, by affecting flow in the liquid powder layer, the rate of powder consumption into the gap between the shell and the mold, and the formation of oscillation marks. The liquid steel solidifies against the four walls of the water-cooled copper mold, and forms a steel shell that must be thick and strong enough to contain the liquid as it is withdrawn continuously from the mold.

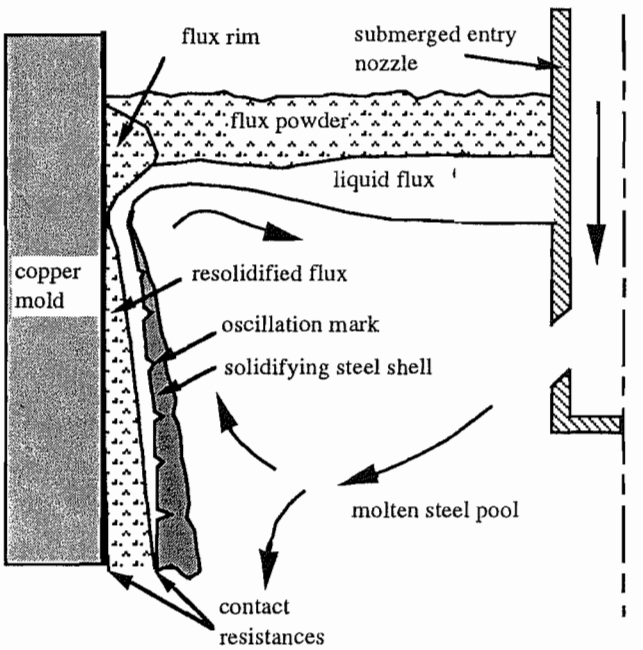

Fig. 1. Schematic of continuous casting process showing flux layers (not to scale)

Mold powder added to the free surface of the liquid steel melts and flows between the steel shell and the mold wall to act as a lubricant, so long as it remains liquid. In addition, the solid and liquid layers of mold flux comprise a large resistance to heat removal. Shrinkage of the steel shell away from the mold walls may generate contact resistances or air gaps, which act as a further resistance to heat flow. The latter

depends on the tendency of the grade to "ripple" (forming an uneven, non-flat surface with deep oscillation marks on solidification), the strength of the shell relative to ferrostatic pressure, mold taper, and mold distortion. These interfacial resistances are the most important factor controlling the rate of heat flow in the process.

Finally, the flow of cooling water through vertical slots in the copper mold withdraws the heat and controls the temperature of the copper mold walls. If the "cold face" of the mold walls becomes too hot, boiling may occur, which reduces heat transfer and makes it more variable. It is clear that many diverse phenomena simultaneously control the complex, dynamic sequence of events, which govern heat transfer in the continuous casting mold.

The present work was undertaken to develop a fast, simple, and flexible model of heat transfer in the mold and shell and related phenomena. All of the above-mentioned phenomena affecting heat flow are included, as each may be of critical significance in a particular circumstance. In particular, the model focuses on a detailed treatment of the gap, which is the most important thermal resistance. The model includes a mass, momentum and heat balances on the flux layer(s) in the interfacial gap.

This model is part of a larger comprehensive system of models of fluid flow, heat transfer, and stress, which is being developed to understand and investigate the formation of defects in the mold. These models include the effects of mold distortion,[2] the influence of fluid flow in the liquid pool on solidification of the shell,[3] and coupling between the thermal / mechanical behavior of the shell and the reduction of heat transfer across the interface due to air gap formation.[4]

The present paper briefly describes the formulation of this model, which has been implemented into a user-friendly FORTRAN program on a personal computer. Validation of the model and several example applications are discussed.

2. PREVIOUS WORK

Many mathematical models have been developed of the continuous casting process, which are partly summarized in a previous literature review.[5] Many of these models are very sophisticated (even requiring supercomputers to run) so are infeasible for use in an operating environment. Of the remaining models which consider the mold, most simulate either solidification of the shell, or heat conduction through the mold. There is usually a simplified treatment of the interfacial gap, despite its known importance.

A few models have considered more detailed treatment of the powder layers in the gap.[6] These models have generally oversimplified the shell and mold. There appears to be a need for a comprehensive model of the shell, mold, and gap, that is fast and easy to run, for use at the plant.

3. MODEL FORMULATION

The present model consists of 2-D steady-state heat conduction within the mold, coupled with 1-D transient heat flow through the solidifying steel shell, as it moves down through the mold. The model simulates axial behavior down a chosen position on the mold perimeter. Mid-wideface and mid-narrow face simulations can thus be conducted separately. A brief description of the model is given here, as further details are provided elsewhere.[7,8]

3.1. Heat Conduction in the Solidifying Steel Shell

Temperature in the thin solidifying steel shell is governed by the 1-D transient heat conduction equation, which includes grade- and temperature-dependent thermal properties:

$$\rho C_p^* \frac{\partial T}{\partial t} = k\frac{\partial^2 T}{\partial x^2} + \frac{\partial k}{\partial T}\left(\frac{\partial T}{\partial x}\right)^2 \qquad (1)$$

where $C_p^* = C_p \dfrac{\Delta H_L}{T_{liq} - T_{sol}}$

and ρ = steel density (kg m^{-3})
C_p= steel specific heat (J kg^{-1} K^{-1})
k = steel thermal conductivity (W m^{-1} K^{-1})
T = temperature (°C)
x = shell thickness direction (m)
ΔH_L = steel latent heat of fusion (J kg^{-1})
T_{liq} ,T_{sol} = liquidus, solidus temps (°C)

This equation assumes that axial (z) heat conduction is negligible in the steel, (due to the large advection component) and that latent heat is evolved linearly between the solidus and liquidus temperatures. The simulation domain is a slice through the liquid steel and solid shell pictured in Fig. 2 together with the boundary conditions. The boundary condition on the external surface of the shell imposes the heat flux lost to the interfacial gap, q_{int}, which depends on the behavior of the flux layer, described in detail later. The internal solid / liquid steel interface incorporates the "superheat flux" delivered from the turbulent liquid pool, described next.

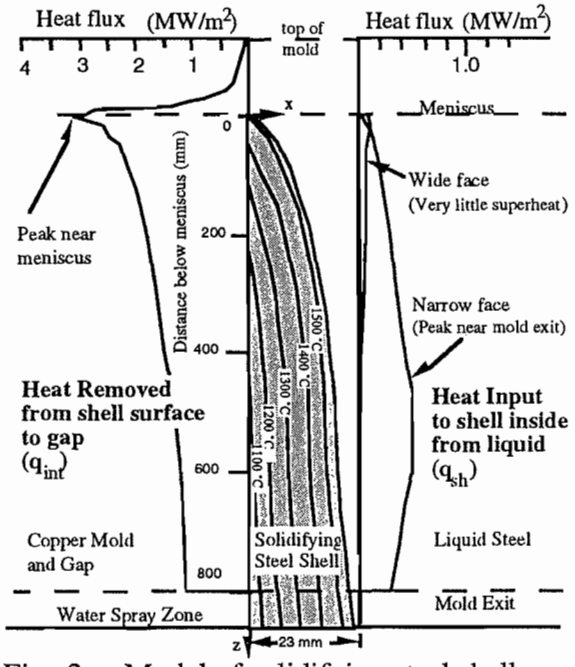

Fig. 2. Model of solidifying steel shell showing typical isotherms and heat flux conditions (CON1D)

3.2. Superheat Delivery

Before it solidifies, the steel must first cool from its initial pour temperature to the liquidus temperature. Due to turbulent convection in the liquid pool, the "superheat" contained in this liquid is not distributed uniformly. A small database of results from a 3-D fluid flow model[3] is used to determine the heat flux delivered to the solid / liquid interface due to the superheat dissipation, as a function of distance below the meniscus, q_{sh}. Examples of this function are included in Fig. 2, which represents results for a typical bifurcated, downward-directing nozzle. The initial condition on the liquid steel at the meniscus is then simply the liquidus temperature.

This superheat function incorporates the variation in superheat flux according to the superheat temperature difference, ΔT_{sup}, casting speed, V_c, and nozzle configuration. The influence of this function is insignificant to shell growth on most of the wide face, where superheat flux is small and contact with the mold is good.

3.3. Heat Conduction in the Mold

Two dimensional, steady state temperatures within a rectangular vertical section through the upper portion of the mold are calculated by solving:

$$k_m\left(\frac{\partial^2 T}{\partial x^2}+\frac{\partial^2 T}{\partial z^2}\right)=0 \qquad (2)$$

where k_m = mold thermal conductivity ($Wm^{-1}K^{-1}$)
T = temperature (°C)
x = shell thickness direction (mm)
z = casting direction (mm)

Below the meniscus region, (generally chosen to extend from the top of the mold to 50 mm below the meniscus), heat flow is almost one dimensional. Heat flow through the mold is then characterized simply by:

$$T_{hotc}=T_{water}+q_{int}\left(\frac{1}{h_{water}}+\frac{d_m}{k_m}\right) \qquad (3)$$

where T_{hotc} = mold surface temperature (°C)
T_{water} mold cooling water temperature (°C)
q_{int}= shell/mold interface heat flux (Wm^{-2})
h_{water}= effective mold / water h ($Wm^{-2}K^{-1}$)
d_m = mold wall thickness (m)
k_m = mold thermal conductivity ($Wm^{-1}K^{-1}$)

The two model domains are included in Fig. 3 a). The calculation requires, as boundary conditions, q_{int}, T_{water}, and h_{water}.

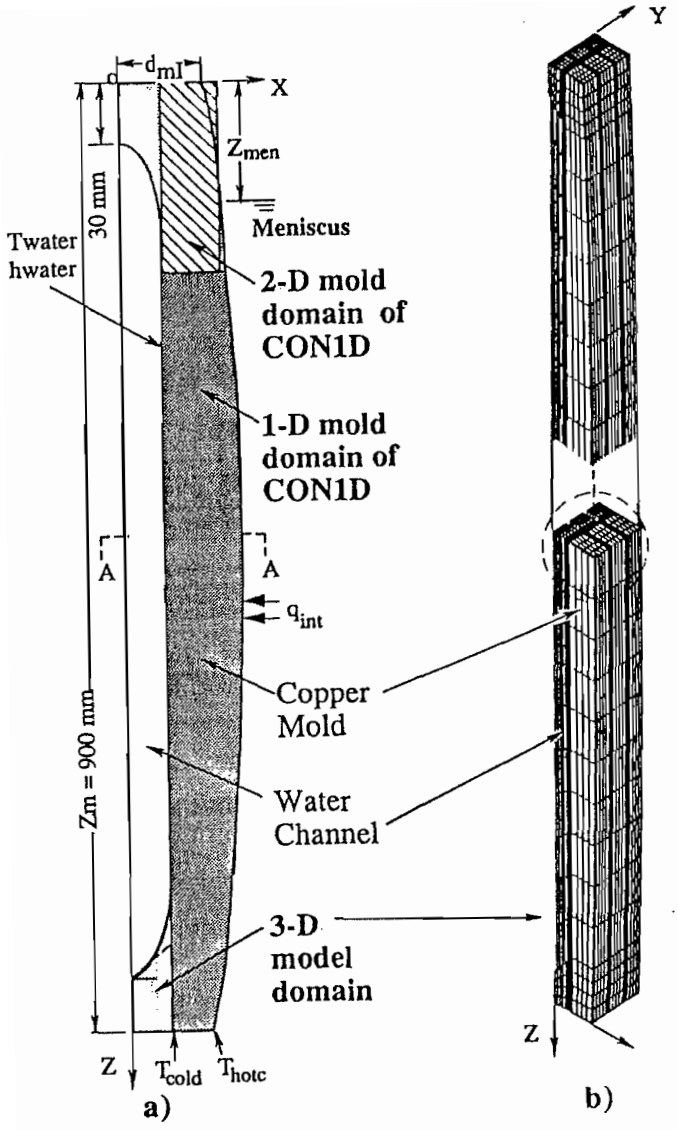

Fig. 3. a) 2-D and 1-D CON1D model domains superimposed on 3-D curved mold section
b) Finite element mesh for 3-D mold analysis

3.4. Convection to the Cooling Water

The effective heat transfer coefficient between the cooling water and the cold face ("water-side") of the mold, h_{water}, is calculated including a possible resistance due to scale deposits on the surface of the cooling water channels:

$$h_{water} = \frac{1}{\frac{d_{scale}}{k_{scale}} + \frac{1}{h_{fin}}} \qquad (4)$$

where h_{water} = effective mold / water h ($Wm^{-2}K^{-1}$)
d_{scale} = scale layer thickness (m)
k_{scale} = scale layer conductivity ($Wm^{-1}K^{-1}$)
h_{fin} = mold cold face h ($W\ m^{-2}\ K^{-1}$)

To account for the complex nature of heat flow in the undiscretized width direction, the heat transfer coefficient between the mold cold face and the cooling water, h_{fin}, treats the sides of the water channels as heat-transfer fins.

$$h_{fin} = \frac{h_w\, w_{ch}}{L_{ch}} + \frac{\sqrt{2h_w\, k_m (L_{ch}-w_{ch})}}{L_{ch}} \tanh \sqrt{\frac{2h_w\, d_m}{k_m (L_{ch}-w_{ch})}} \qquad (5)$$

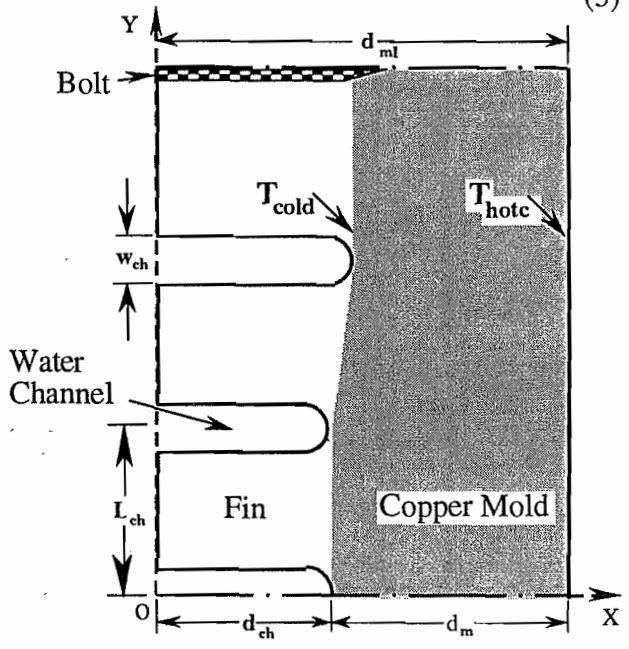

Fig. 4. Horizontal section through mold

where h_{fin} = mold cold face h ($W\ m^{-2}\ K^{-1}$)
h_w = mold surface / water h ($W\ m^{-2}\ K^{-1}$)
w_{ch} = cooling water channel width (mm)
L_{ch} = cooling water channel thickness (mm)
k_m = mold thermal conductivity ($Wm^{-1}K^{-1}$)
d_m = mold wall thickness (mm)

where the geometry parameters, L_{ch}, w_{ch}, d_m, d_{ch} are shown in Fig. 4. The heat transfer coefficient between the water and the sides of the water channel, h_w, is calculated assuming turbulent flow through an equivalent-diameter pipe.[9]

This equation assumes that the base of the water slot has constant temperature, so is most

accurate for closely-spaced slots. The presence of the water slots can either enhance or diminish the heat transfer relative to a mold with constant thickness, d_m. Deep, closely-spaced slots augment the heat transfer coefficient, (h_{fin} larger than h_w) while shallow, widely-spaced slots inhibit heat transfer. In most molds, h_{fin} and h_w are very close.

3.5. Heat Transfer Across the Interfacial Gap

Heat transfer across the interfacial gap governs the heat flux leaving the steel, q_{int}, to enter the mold. To calculate this at every position down the mold, the model evaluates an effective heat transfer coefficient, h_{gap}, between the surface temperatures of the steel shell, T_s, and the hot face of the mold wall, T_{hotc}:

$$q_{\text{int}} = h_{gap}(T_s - T_{hotc}) \qquad (6)$$

$$h_{gap} = \frac{1}{\left(\frac{d_a}{k_a} + \frac{d_s}{k_s} + \frac{d_l}{k_l} + \frac{d_{oeff}}{k_{oeff}}\right)} + h_{rad}$$

where q_{int}= shell/mold interface heat flux (Wm^{-2})
h_{gap}= shell/mold gap effective h ($Wm^{-2}K^{-1}$)
T_s = steel surface temperature (°C)
T_{hotc} = mold surface temperature (°C)
d_a, d_s, d_l, d_{oeff} = thickness of the air gap, solid, liquid flux, and oscillation mark layers
k_a, k_s, k_l, k_{oeff} = conductivity of the air gap, solid, liquid flux, and oscillation mark layers
h_{rad}=radiation effective h ($Wm^{-2}K^{-1}$)

Heat conduction depends on the thermal resistances of four different layers of materials contained in the gap. These depend on the time-averaged thickness profiles down the mold of the different layers and their corresponding thermal conductivities. The most important resistances are usually the flux layers, whose thicknesses are calculated as described in the next section.

The equivalent air gap, d_a, is specified as input data and includes contact resistances at the flux / shell and flux / mold interfaces. It may also include a gap due to shrinkage of the steel shell, which is calculated using a separate thermal-stress model.[4] The shrinkage gap is affected by the mold taper and also by mold distortion, which can be calculated by another model.[2] This gap is important when simulating down positions near the corner.

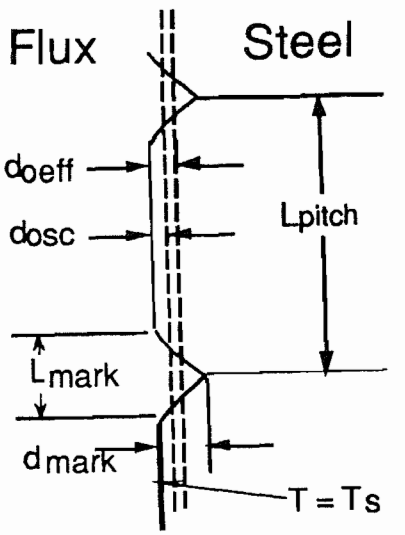

Fig. 5. Model treatment of oscillation marks viscosity/temperature curve.[10]

Non-uniformities in the flatness of the shell surface are incorporated into the model through the prescribed average depth, d_{mark}, and width, L_{mark}, of the oscillation marks, as pictured in Fig. 5.

The oscillation marks affect the thermal resistance in two different ways. Firstly, they reduce heat conduction by providing an extra gap, represented by the effective average depth of the marks, d_{oeff}:

$$d_{oeff} = \frac{0.5\ L_{mark} d_{mark}}{(L_{pitch} - L_{mark})\left(1 + 0.5\frac{d_{mark}}{(d_s + d_l)}\frac{k_f}{k_{mark}}\right) + L_{mark}} \qquad (7)$$

where
d_{oeff} = effective osc. mark depth (mm)
d_{mark} = max. osc. mark depth (mm)
L_{mark} = width of oscillation marks (mm)
L_{pitch}= ratio of the casting speed to the oscillation frequency, freq (mm)
d_s, d_l, thickness of solid, liquid flux layers
k_{mark}=osc. mark conductivity ($Wm^{-1}K^{-1}$)
k_f= conductivity of rest of gap ($Wm^{-1}K^{-1}$)

This gap is assumed to be filled with either flux or air, depending on the local shell temperature. Secondly, the oscillation marks consume mold flux, so affect the behavior of the flux layer thicknesses, as described in the next section.

When the gap is large, significant heat is transferred by radiation across the semi-transparent flux layer.

$$h_{rad} = \frac{m^2 \sigma \left(T_s^2 + T_{hotc}^2\right)\left(T_s + T_{hotc}\right)}{0.75\ a\ \left(d_l + d_s\right) + \frac{1}{\varepsilon_s} + \frac{1}{\varepsilon_m} - 1} \quad (8)$$

where h_{rad}=radiation effective h ($Wm^{-2}K^{-1}$)
m= flux refractive index
σ = Stefan Boltzman constant ($Wm^{-2}K^{-4}$)
T_s = steel surface temperature (°C)
T_{hotc} = mold surface temperature (°C)
a = flux absorption coefficient (m^{-1})
d_s, d_l = thickness of solid, liquid flux layers (m)
ε_s, ε_m = steel, mold surface emmisitivities

Below the mold, heat flux is applied as a function of spray cooling practice (based on water flux), natural convection, and heat conduction to the rolls. This enables the model to simulate the entire continuous casting process, if desired.

3.6. Mass and Momentum Balance on Powder Flux Layers

Flux is assumed to flow down the gap as two distinct layers: solid and liquid. The solid layer is assumed to move at a time-average velocity, V_s, which is always greater than zero and less than the casting speed, V_c, according to the input factor, f_s.

$$V_s = f_s\ V_c \quad (9)$$

where: V_s = velocity of solid flux (mm s^{-1})
f_s = empirical flux speed factor $(0 < f_s < 1)$
V_c = casting speed (mm s^{-1})

Velocity in the liquid layer is governed by the simplified Navier-Stokes equation:

$$\frac{\partial}{\partial x}\ \mu \frac{\partial v_z}{\partial x} = (\rho_{Fe} - \rho_{flux})\ g \quad (10)$$

where: μ = flux viscosity (Pa-s)
v_z = velocity in casting direction (m s^{-1})
x = shell thickness direction (m)
ρ_{Fe} = steel density (kg m^{-3})
ρ_{flux} = flux density (kg m^{-3})
g = gravity (m s^{-2})

A small body force opposing flow down the wide face is created by the difference between the ferrostatic pressure from the liquid steel, ρ_{Fe} g, and the average weight of the flux, ρ_{flux} g.

The casting speed is imposed at the point of contact between the shell and the liquid layer, which is assumed to flow in a laminar manner, owing to its high viscosity. The viscosity of the molten flux, $\mu(T)$, is assumed to vary exponentially with distance across the gap, according to the temperature:

$$\mu = \mu_o \left(\frac{T_o - T_{fsol}}{T - T_{fsol}} \right)^n \quad (11)$$

where: μ =flux viscosity (Pa-s)
μ_0 = flux viscosity at T_o (Pa-s)
T_o = reference temp (usually 1300°C)
T_{fsol}= flux solidification temperature (°C)
n = empirical flux viscosity exponent

where the parameters T_{fsol} and n are chosen empirically to fit the measured data. An example of the good fit obtained with this function is given in Fig. 6, for typical measured viscosities.[10]

Equations 9-11 yield a velocity distribution across the flux layers, which is illustrated in Fig. 7. Integrating across the liquid region yields an average velocity for the liquid layer, V_l:

$$V_l = \frac{V_c + V_s(n+1)}{n+2} + \frac{\left(\rho_{Fe} - \rho_{flux}\right) g\ d_l^2}{\mu\left(T_s'\right)(n+2)^2(n+3)} \quad (12)$$

where V_l = avg. velocity of liquid flux (m s^{-1})
V_c = casting speed (m s^{-1})
V_s = velocity of solid flux (m s^{-1})
n = flux viscosity exponent
ρ_{Fe} = steel density (kg m^{-3})
ρ_{flux} = flux density (kg m^{-3})
g = gravity (9.81 m s^{-2})
d_l = thickness of liquid flux layer (m)
μ = flux viscosity (Pa-s)
T_s' = steel outside surface temp. (°C)

Mass balance was imposed to express the fact that the known powder consumption, Q_f (kg m^{-2}), controls the total powder flow rate past every location down the interfacial gap. Flux can be carried by the solid layer, liquid layer, or in the oscillations marks:

$$\frac{Q_f V_c}{\rho_{flux}} = V_s d_s + V_l d_l + V_c d_{osc} \qquad (13)$$

where: Q_f = mold flux consumption (kg m^{-2})
V_c = casting speed (m s^{-1})
ρ_{flux} = flux density (kg m^{-3})
V_s = solid flux velocity Eq. 9 (m s^{-1})
V_l = liquid flux velocity Eq. 12 (m s^{-1})
d_s, d_l, thickness of solid, liquid flux layers
d_{osc} = effective mark thickness (volume)

The average depth of the oscillation marks (regarding their volume to carry flux), d_{osc}, is calculated from:

$$d_{osc} = \frac{0.5\, L_{mark}\, d_{mark}}{L_{pitch}} \qquad (14)$$

where: d_{osc} = effective mark thickness (mm)
L_{mark} = width of oscillation marks (mm)
d_{mark} = max. osc. mark depth (mm)
L_{pitch} = V_c / freq (mm)

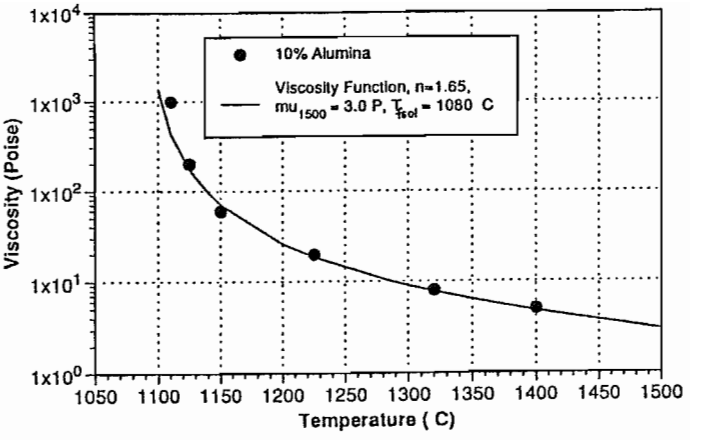

Fig. 6. Comparison of measured and fitted viscosity/temperature curve

Two different regions can be distinguished down the mold, according to the lubrication condition. Close to the meniscus, the first region includes a liquid flux layer, which remains present so long as the outer surface temperature of the steel T_s' exceeds the flux solidification temperature, T_{fsol}. The liquid layer thickness is calculated by assuming a linear temperature profile across each layer in the gap (see Fig. 7).

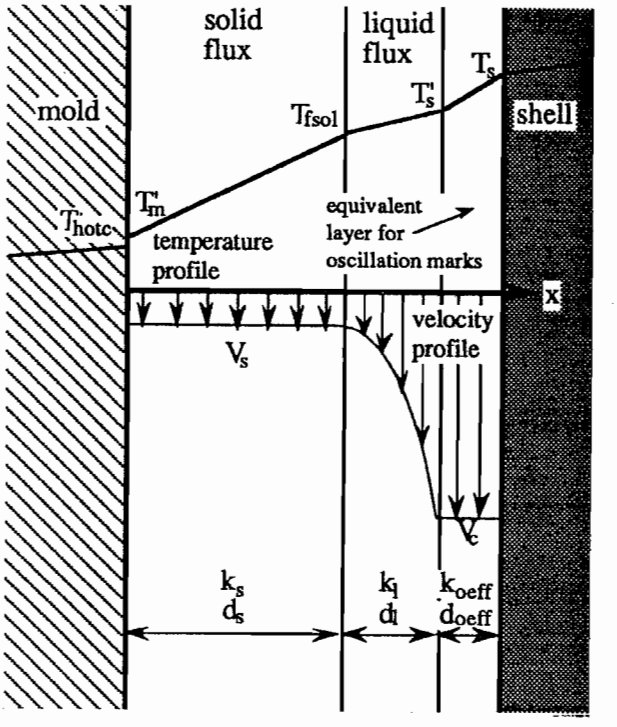

Fig. 7. Velocity and temperature profiles assumed across interfacial gap

Flux in the oscillation marks remains liquid longer, due to the higher local shell temperature at their roots, T_s. Once the oscillation marks cool below the flux solidification temperature, however, the flux entrapped in them solidifies. This defines the second region, which consists of totally solid flux, moving downward at the uniform speed, V_s. The oscillation marks no longer transport flux, so become filled with air.

3.7. Solution Methodology

The model requires simultaneous solution of three different systems of equations: 1-D transient heat conduction and solidification of the steel shell, 2-D steady state heat conduction in the mold, and the equations balancing heat, mass and momentum in the gap. The equations are solved by first performing a transient 1-D simulation of the shell, gap and mold. The model uses an explicit, central-finite difference algorithm, which limits the maximum time step size, Δt. The results are used as initial conditions for the 2-D mold calculation, which is solved analytically, relating distance down the mold, z, to time in the shell through the casting speed. Subsequently, the model iterates between the 1-D shell and 2-D mold calculations until convergence is achieved. This produces a self-consistent prediction, which is stable for all coupled simulations investigated and converges in 3-4 iterations.

The model has been incorporated into a user-friendly FORTRAN program, CON1D. The program requires less than 500 KBytes of memory and runs on a personal computer in less than 1 minute.

4. MODEL VERIFICATION

The internal consistency and accuracy of the modeling assumptions have been verified through comparison with known solutions. The solidification model was able to match analytical solutions for metal-controlled solidification.[11]

The model was next compared with results from 3-D ABAQUS calculations on a realistic representation of a segment of a typical casting mold, including mold curvature, rounded water slots of varying length and width, and bolts. The finite element mesh used in the ABAQUS simulations is included in Fig. 3b).

The same conditions were imposed in each model, including the heat flux profile, q_{int}, included in Fig. 2. Fig. 8 shows the remarkable agreement between the 3-D and 1-D models. This suggests that the fin assumption used in CON1D is valid.

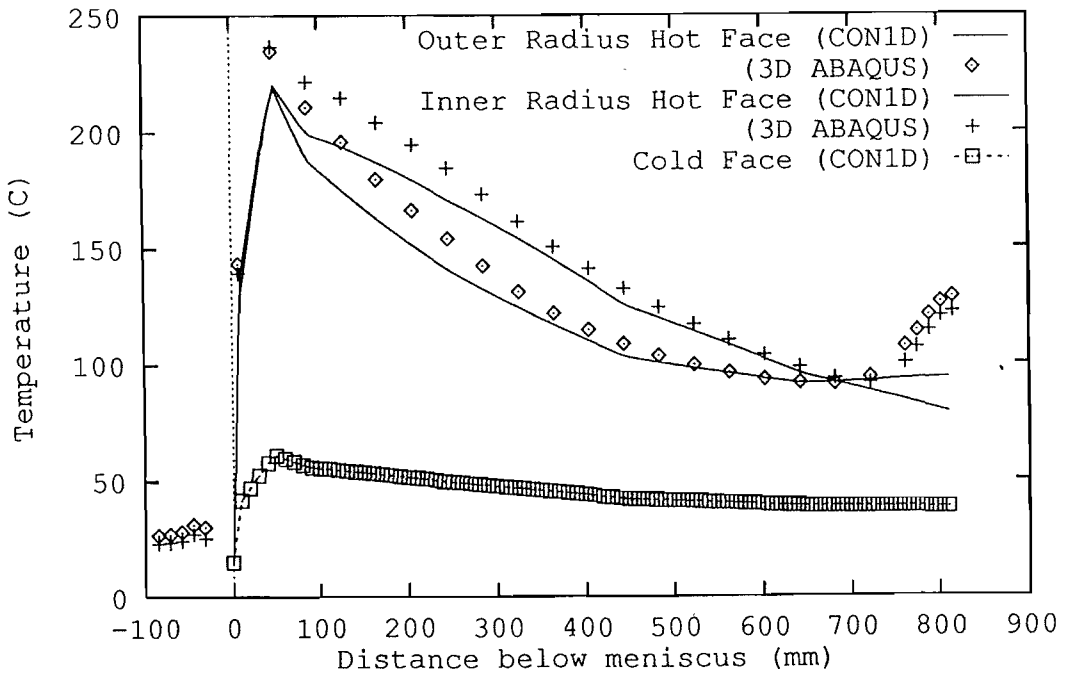

Fig 8. Comparison between CON1D and 3D- ABACUS mold temperature calculations

Fig. 8 also illustrates the effect of mold wall curvature on the temperature distribution. This is accounted for in CON1D by varying the wall thickness down the mold according to the radius of curvature, R_I. The effect is seen to range from practically none at the meniscus, where inner and outer radius wall thicknesses are almost equal, to a maximum of 30 °C midway down the mold.

At mold exit, the 3-D model shows that temperature increases about 50 °C due to the end of the water slots. This increase occurs despite a continuously decreasing q_{int}. This effect is naturally not predicted by the simple CON1D model. Thus, care must be taken when interpreting thermcouple measurements made near mold exit.

5. MODEL CALIBRATION

Although the model has been shown to be accurate, it cannot be used quantitatively until it is calibrated to match measurements on the specific operating caster of interest. This step is necessary because so many of the inputs to the model are uncertain.

To date, the model has been calibrated to match several different casters, including BHP LPD in Whyalla, South Australia; BHP RBPD in Newcastle, New South Wales; New Zealand Steel in Aukland, NZ; and LTV Steel in Cleveland, OH. In order to calibrate the model, it is simply run several times, using trial and error to find values of the model parameters that allow the model predictions to match all of the known measurements. Those measurements can include the cooling water temperature rise, the time-average temperature of any thermocouples embedded in the mold, the thickness profile of breakout shells, and the thickness of solidified mold powder layers and flux rims.

Specifically, adjustments can be made to the velocity of the solid flux layer, the value of the contact resistances (effective air gap) down the mold, and even the thermal properties of the mold flux. Other input parameters include the powder consumption rate and the average oscillation mark depth and width.

In a slab caster with properly designed taper, there should not be any air gap due to shrinkage down the center of the wide face. This is because ferrostatic pressure pushes the long, wide, weak shell against the mold to maintain as close a contact as possible. This greatly simplifies model calibration when simulating a slice through the wide face of the mold and shell.

This next sections report on the calibration and results of simulations performed for conditions given in Table 1. The input parameters were calibrated to match the casting conditions of several different 0.225 x 1.78 m slabs of 0.05 %C steel cast at LTV Steel Cleveland, OH, where mold thermocouple temperatures and other measurements were available.

5.1. Mold Cooling Water Temperature Rise

The measured average rate of heat flux extracted from the mold, Q, should match that calculated by the model via:

$$Q = \frac{V_c}{Z_{mold}} \sum_{Z_{mold}} q_{\text{int}} \Delta t \qquad (15)$$

where: Q = average mold heat flux (kW/m^2)
V_c = casting speed ($mm\ s^{-1}$)
Z_{mold} = working mold length (mm)
q_{int} = shell/mold interface heat flux (Wm^{-2})
Δt = time step size (s)

This heat transfer rate is readily inferred from the temperature increase of the mold cooling water, ΔT_{water}, which is also calculated:

$$\Delta T_{water} = \sum_{mold} \frac{q_{\text{int}} L_{ch} V_c \Delta t}{\rho_w C_{pw} V_w w_{ch} d_{ch}} \qquad (16)$$

where: ΔT_{water}= cooling water temp. rise (°C)
q_{int} = shell/mold interface heat flux (Wm^{-2})
L_{ch} = cooling water channel thickness (m)
V_c = casting speed ($m\ s^{-1}$)
Δt = time step size (s)
ρ_w, C_{pw} = water density, specific heat

V_w = cooling water velocity (m s^{-1})
w_{ch} = cooling water channel width (m)
d_{ch} = cooling water channel depth (m)

This equation assumes that the cooling water slots have uniform rectangular dimensions, w_{ch} and d_{ch}, and spacing, L_{ch}. Heat entering the hot face (between two water channels) is assumed to pass entirely through the mold to heat the water flowing through the cooling channels. The prediction must be modified to account for missing slots due to bolts or water slots which are beyond the slab width, so do not participate in heat extraction.

5.2. Mold Temperatures

Fig. 9 shows an example comparison between the predicted and measured temperatures at several locations down the LTV mold. The agreement indicates the calibration of the model for these typical casting conditions. This figure also shows the predicted hot face and cold face temperature profiles. The sudden change in temperature is due to a sudden increase in water channel depth, produced by experimental inserts used in the trial.

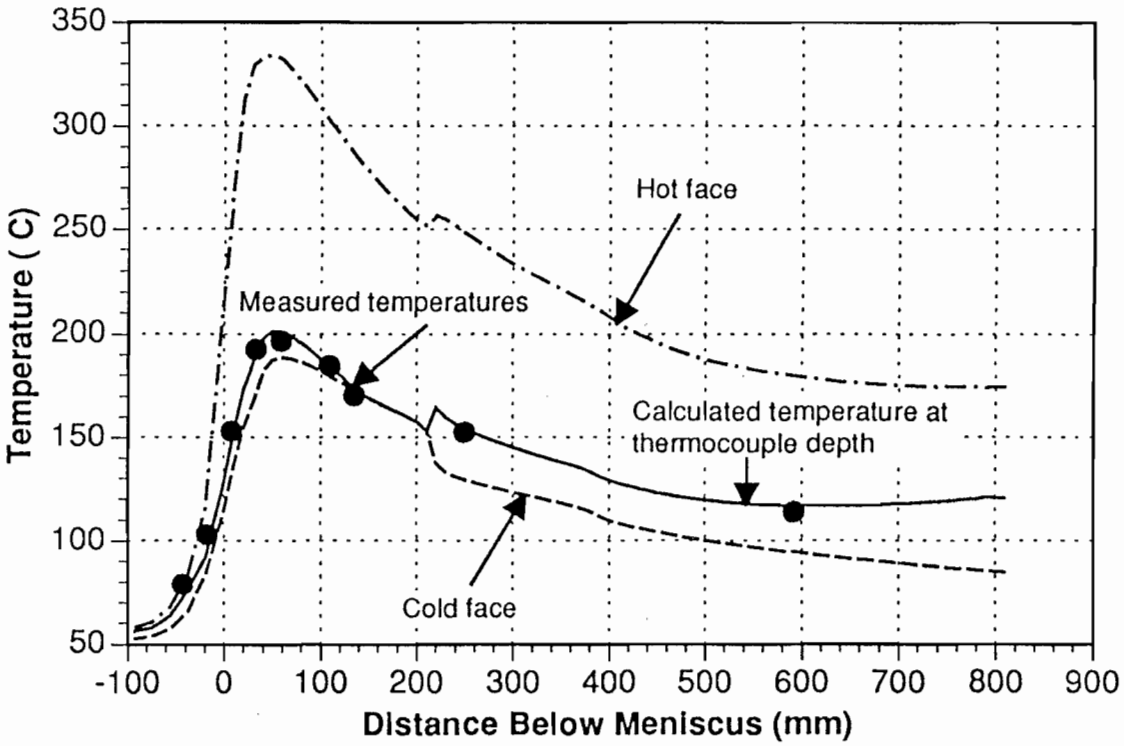

Fig. 9. Comparison between CON1D calculated and measured mold temperatures

These predictions are useful for calibration of the model with an operating caster. For the LTV mold, the predicted cooling water temperature rise of 8.9 °C matches the measured rise.

5 3. Shell Thickness

Fig. 10 compares the predicted shell thickness profile with measurements down a breakout shell. Shell thickness is defined in the model by linearly interpolating the position between the liquidus and solidus isotherms corresponding to the specified solid fraction, f_{sol}.

Growth of the shell naturally depends upon the combination of the interfacial and superheat fluxes. The superheat distribution is important as Fig. 2 shows that the two curves are of the same magnitude in the lower regions of the mold near the narrow face where the hot molten steel jet impinges against the solidifying shell.

Variation in the superheat flux is critical to shell growth down the narrow face and off-corner regions, where problems such as inadequate taper can produce significant air gap(s). Together, the large superheat combined with decreased heat transfer across the interfacial gap can reduce shell growth enough to cause breakouts. This has been the subject of a significant study using the model, which is reported elsewhere.[12]

5.4. Powder Layer Thickness

The model predicts the thickness and velocity profiles expected in the powder layers in the interfacial gap. For example, Fig. 11 shows the solid and liquid flux layer thickness profiles expected for the standard conditions investigated here (Table 1). Unfortunately, no reliable samples could be obtained to validate these results, although the predictions are consistent with findings at other plants.[7]

5.5. Shell Surface Temperature

Typical model predictions of surface temperature of the steel shell are shown in Fig. 12 for the wide face. This prediction can also be used for calibration of the model, if measurements from optical pyrometers located just below mold exit are available.

6. SAMPLE APPLICATIONS

The calibrated model has many applications for both design and operation of continuous casting molds. Firstly, it can help investigate the effect of various process conditions on the fundamentals of mold heat transfer. Most parameters, such as oscillation practice, powder type, casting speed, and steel grade, affect heat transfer in several different ways, which can be isolated and quantified independently.

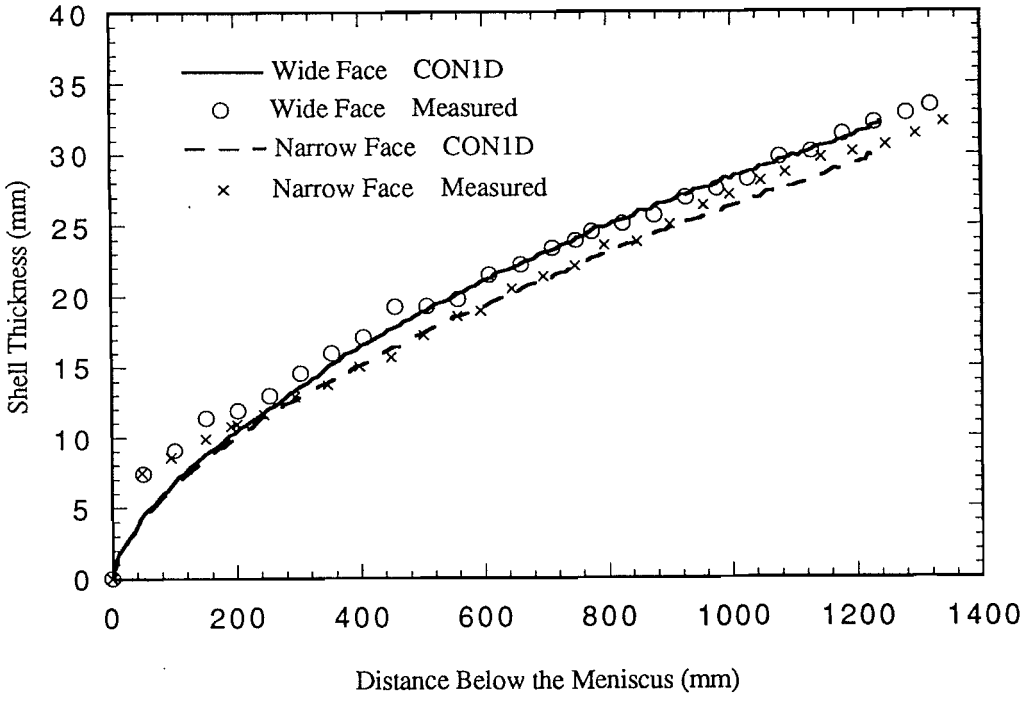

Fig. 10. Comparison between CON1D calculated thickness profile and measurements from breakout shell

The model is being extended to make predictions of potential quality problems, which have more relevance in practice. These include possible warnings of cooling water boiling, breakout danger, excessive mold friction, and crack formation. Finally, the model should predict optimum casting conditions to avoid problems, whenever possible. Initial features of the model toward this goal include a prediction of ideal mold taper.

Increasing casting speed, at constant powder consumption, is seen to increase heat flux over the bottom portion of the mold. This is because the shell is thinner and hotter with the larger casting speed, owing to less time for solidification. The thinner shell provides less resistance to heat flow. The effect diminishes with distance up the mold because the resistance of the thinner shell is always relatively small.

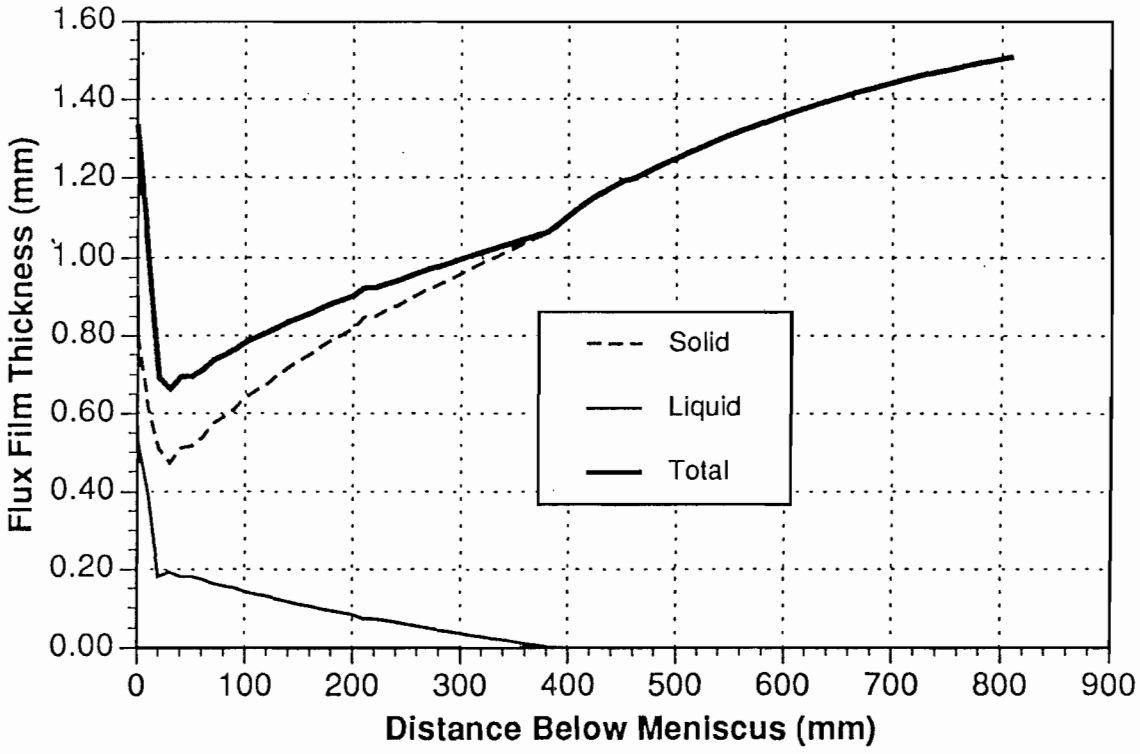

Fig. 11 Calculated flux layer thickness profile

6.1. Parametric Studies

As an example of the use of the model to understand fundamental phenomena in the mold, simulations were performed to investigate just two of the many interdependent parameters: casting speed and mold powder consumption. Fig. 13 presents the heat flux profiles down the mold calculated for two different casting speeds and powder consumption rates. The realistic conditions are the standard case in Table 1 (V_c=1.0 m/min and Q_f=0.6 kg/m^2) and the higher casting speed (1.25 m/min) with the lower consumption rate (0.5 kg/m^2).

Decreasing powder consumption rate, at constant casting speed is seen to increase heat flux in the top portion of the mold. This is because the average thickness of the flux layers decreases, thus lowering the interfacial resistance. The effect diminishes with distance down the mold.

In practice, increasing casting speed is accompanied by a simultaneous decrease in powder consumption rate. The net result, given in Fig. 13, is to increase heat flux almost uniformly down the entire length of the mold. This is reflected in uniformly higher mold hot face temperatures, as seen in the model predictions in Fig. 14, which match the measurements.

The model is suited to fundamental parametric studies of this kind. For example, steel grade affects the average oscillation mark size, powder consumption rate, air gap size due to thermal contraction (narrow face), and steel strength. Mold powder properties and oscillation practice have similar interdependent effects.

6.2. Boiling Prediction

If the mold cold face temperature exceeds the boiling temperature for the given operating pressure in the cooling water channels, then the model issues a warning that boiling is possible. Boiling in the water channels lowers the rate of heat removal and causes temperature fluctuations that together pose a serious potential quality problem. Fig. 8 shows that boiling is not expected to be a problem for the conditions investigated here. Adding a 0.02 mm thick layer of scale on the mold cold face, however, is predicted to raise the cold face temperature into the danger range. On the other hand, adding a 0.5 mm thick protective Ni coating to the hot face is predicted to have a negligible effect on heat flux and raises cold face temperature less than 15 °C. The model is ideal for quantifying these effects.

6.3. Breakout Analysis

The model can be used to understand how a breakout may have arisen. Sticker breakouts are easily identified by their characteristic effect on mold thermocouple histories. Other breakouts, such as those caused by inadequate taper, can be more difficult to understand. For example, the model could be used to determine whether a given narrow-face breakout was more likely caused by excessive superheat resulting from a clogged nozzle, or from insufficient mold taper, causing an excessive gap. Either condition could produce a narrow-face shell that is too hot and thin to have the hot strength needed to avoid rupture. Further calibration may allow the model to accurately warn of a potential breakout when shell growth is predicted to fall below specified critical values.

6.4. Lubrication Prediction

The model is being extended to predict the consequences of interfacial heat transfer on steel quality. If the mold flux, which fills most of the gap, is allowed to cool completely below its crystallization temperature, then it becomes viscous and is less able to lubricate the strand. This may increase mold friction and transient temperature changes, making problems such as surface cracks more likely. Fig. 11 predicts this could occur below 400 mm, for the present conditions.

6.5. Crack Formation Analysis

The model can be used to locate where defects are formed. For example, by accurately predicting the shell thickness exiting the mold, the model can identify whether a subsurface crack formed in or below the mold. This can be difficult to tell, particularly near the narrow face, where shell growth may be slow. Here, a crack forming below the mold might appear to have formed in the mold without an accurate calculation of shell growth. The model can also simulate phenomena below the mold, such as reheating of the shell surface, which can lead to surface cracks. This is useful for designing spray water cooling systems.

6.6. Calculation of Ideal Mold Taper

The narrow-face of the mold should be tapered to match the shrinkage of steel shell, which is cooling against the wide face. Previous work has determined that this shrinkage depends mainly on the surface temperature of the shell and the steel grade.[4] The model predicts ideal average taper, TP, by:

$$TP = \frac{TLE(T_{sol}) - TLE(T_{s'e})}{Z_{mold}} \qquad (17)$$

where: TP = ideal average mold taper (%/m)
TLE= thermal linear expansion
T_{sol} = steel solidus temperature (°C)
$T_{s'e}$= outer shell temp. at mold exit (°C)
Z_{mold} = working mold length (m)

Here, TLE is the thermal linear expansion function for the given steel grade, calculated from weighted averages of the phases present:

$$TLE = \%\delta \ TLE_{\delta}(T,\%C) + \%\gamma \ TLE_{\gamma}(T,\%C) \qquad (18)$$

where: TLE= thermal linear expansion function
δ = delta-ferrite phase of steel

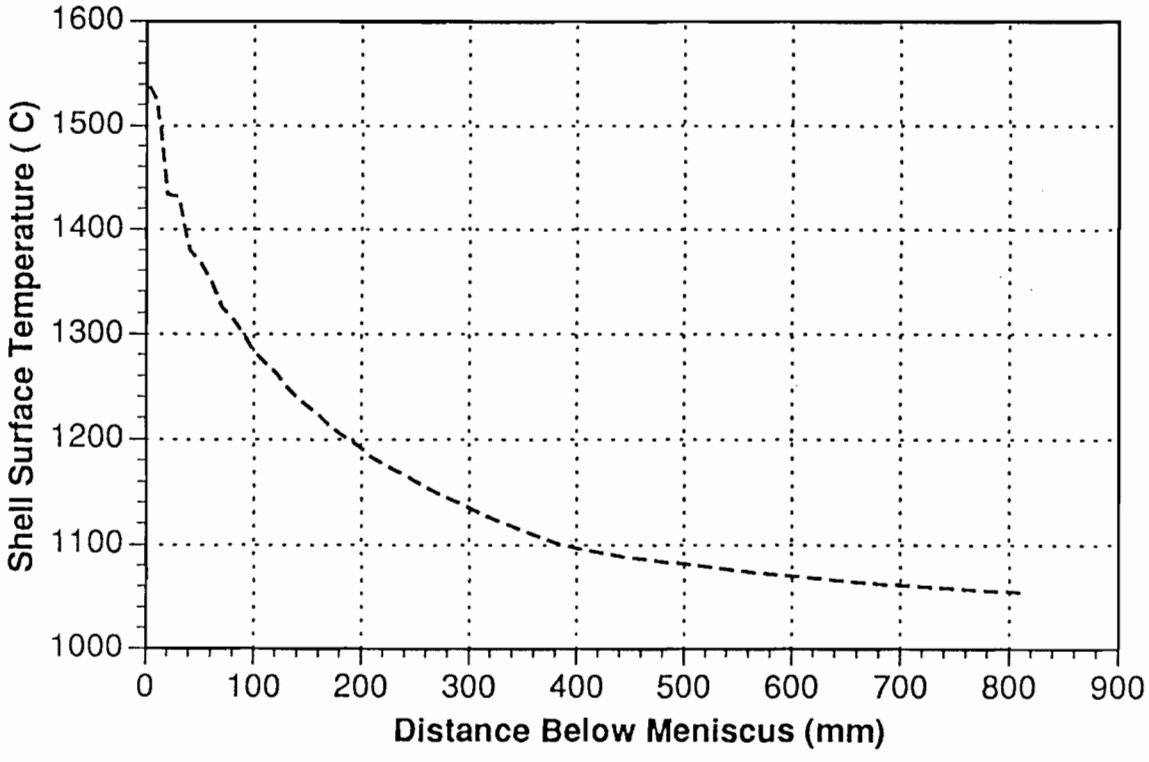

Fig. 12. Calculated steel shell surface temperature

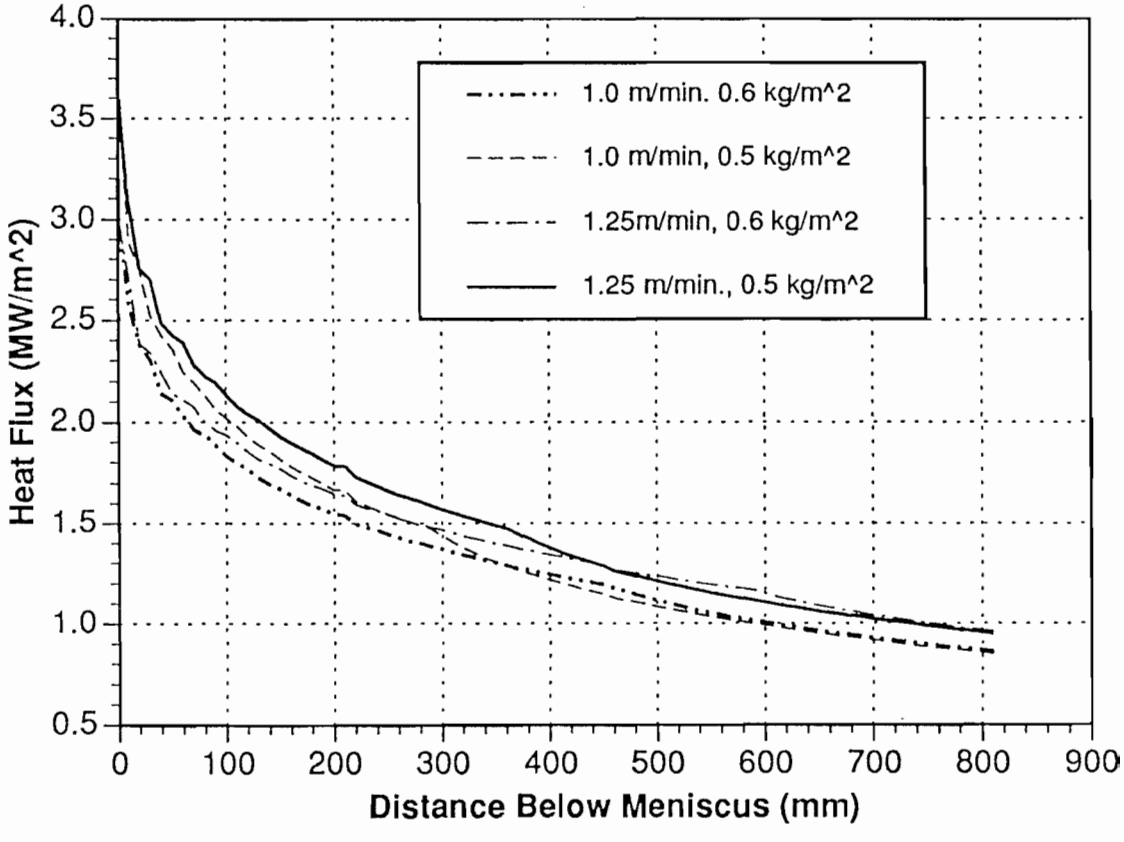

Fig. 13. Effect of casting speed and powder consumption on the heat flux profile

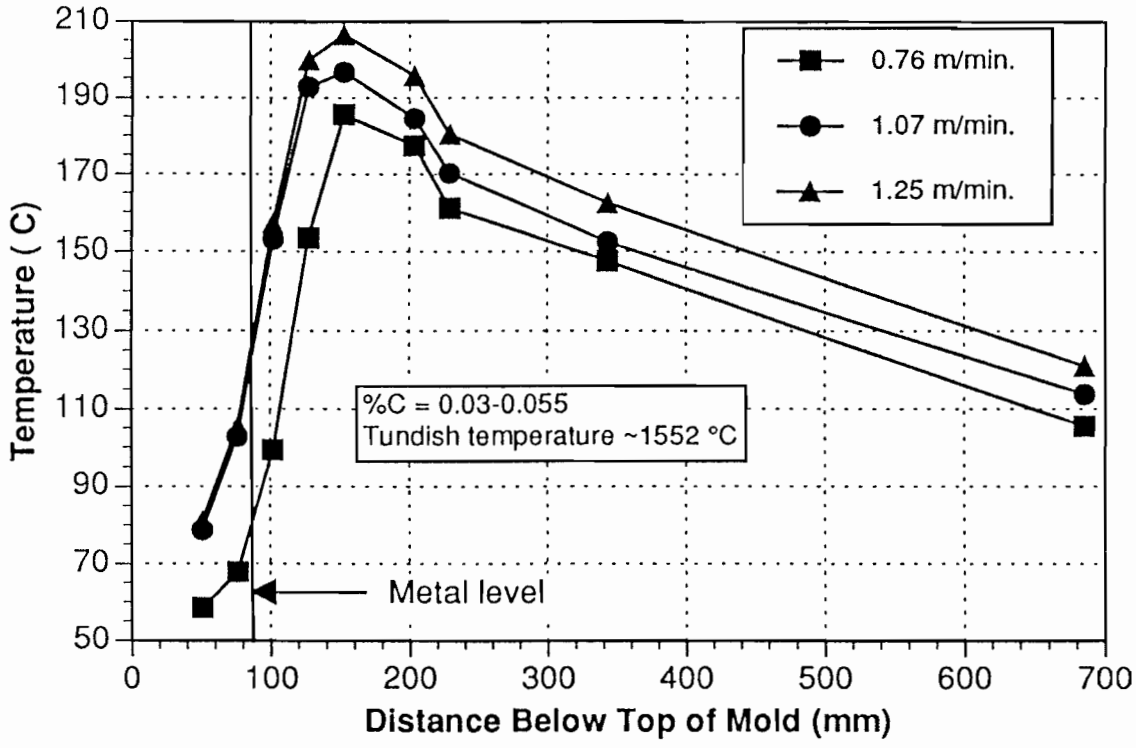

Fig. 14. Effect of casting speed on mold temperature

γ = austenite phase
T = local steel temperature (°C)
C = carbon content
% = percent

Surface temperature depends on many factors, including casting speed, and interfacial heat transfer, which are accounted for in the model. The typical results in Fig. 12 also indicate that the temperature drop of the shell surface is not uniform as it moves down the mold. With a linear taper, the narrow-face shell attempts to shrink away from the upper portion of the mold, while it is pushed against the lower portion of the mold. To match the shrinkage, it is clear that taper should be increased high in the mold and decreased lower down. Mold distortion, viscoplastic creep of the steel, and other factors should also be taken into account when designing a non-linear mold taper. These calculations require sophisticated thermal-stress models, to calculate temperatures, stresses, and shrinkage, including the formation of an air gap near the corners, and its effect on heat flow across the mold / shell interface. The calibrated CON1D model is being used to provide calibrated input data to help quantify the interfacial heat transfer.

6.7. Future Applications

The model is based on conservation laws that must hold, regardless of the complex phenomena present in the caster. However, there are many more unknowns than equations. Thus, the model requires extensive calibration, which include the values of many parameters not currently known. Preferably, some of the required input data should be predicted, such as powder consumption rate and oscillation mark size.

Much further work is needed before the model can realize its full potential as a predictive tool for design, improvement, and control of continuous casting mold operation. For example, the prediction of surface crack formation requires incorporation of transient or local variations in heat transfer, coefficient of friction data, and grade-dependent fracture criteria. This work will require calibration with other, more advanced model calculations, in addition to experimental measurements, and empirical findings.

Table 1. Standard input conditions (wide face inner radius)

a	250 m^{-1}
C_{pw}	4179 J kg^{-1} K^{-1}
d_a	0 mm
d_{ch}	25 mm
$d_m(z=0)$	51 mm
d_{mark}	0.45 mm
d_{scale}	0.010 mm
freq	84 cpm
f_s	17.5 pct
f_{sol}	70 pct
g	9.8 m s^{-2}
k_a	0.06 W $m^{-1}K^{-1}$
k_m	315 W $m^{-1}K^{-1}$
k_s, k_l	1.5 W $m^{-1}K^{-1}$
k_{scale}	0.55 mm
k_w	0.615 $m^{-1}K^{-1}$
L_{ch}	24 mm
L_{mark}	4.5 mm
m	1.5
n	0.85
Q_f	0.60 kg m^{-2}
R_I	11.76 m
ΔT_{sup}	21 °C
T_{liq}	1529 °C
T_{sol}	1509 °C
T_{fsol}	1045 °C
T_o	1300°C
Δt	0.004 s
V_c	1.07 m min^{-1}
V_w	7.8 m s^{-1}
w_{ch}	5 mm
Z_{mold}	810 mm
ΔH_L	272 kJ/kg
ε_s, ε_m	0.5, 0.8
μ_0	0.11 Pa-s = 10 Poise
μ_w	0.00080 Pa-s
ρ_{Fe}	7400 kg m^{-3}
ρ_{flux}	2500 kg m^{-3}
ρ_w	995.6 kg m^{-3}
σ	5.67x10^{-8} $Wm^{-2}K^{-4}$

7. Conclusions

A comprehensive heat flow model of the continuous slab casting mold has been developed. It includes 1-D solidification of the steel shell, dissipation of superheat, movement of the solid and liquid flux layers in the interfacial gap, and 2-D heat conduction through the mold. The model accounts for the effects of oscillation marks on both heat transfer and powder consumption. It also accounts for variations in water slot geometry and steel grade. It is user-friendly and runs quickly on a personal computer. It has been validated through numerical comparisons and calibrated with measurements on operating casters, including cooling water temperature rise, mold thermocouple temperatures, and breakout shell thickness. In addition to heat transfer, the model predicts ideal mold taper, thickness of the solidified flux layers, and potential quality problems due to powder solidification, and boiling in the water channels. It has many potential applications.

Acknowledgments

The authors wish to thank Inland Steel, Armco, BHP Steel, LTV Steel, and the National Science Foundation (Grant # MSS-89567195-PYI) for funding which made this work possible. Special thanks go to Bill Emling and others at LTV Steel for their valuable help providing operating data and experimental measurements.

References

1. F. M. Najjar, B. G. Thomas and D. E. Hershey: "Turbulent Flow Simulations in Bifurcated Nozzles: Effects of Design and Casting Operation", *Metall. Trans. B*, 1995, **26B**, (4), 749-765.

2. B. G. Thomas, G. Li, A. Moitra and D. Habing: "Analysis of Thermal and Mechanical Behavior of Copper Molds during Continuous Casting of Steel Slabs", in *80th Steelmaking Conference Proceedings*, **80,** ISS, Warrendale, PA, Chicago, IL, 1997, 183-201.

3. X. Huang, B. G. Thomas and F. M. Najjar: "Modeling Superheat Removal during Continuous Casting of Steel Slabs", *Metall. Trans. B,* 1992, **23B**, (6), 339-356.

4. A. Moitra and B. G. Thomas: "Application of a Thermo-Mechanical Finite Element Model of Steel Shell Behavior in the Continuous Slab Casting Mold", in *Steelmaking Proceedings*, **76,** Iron and Steel Society, Dallas, TX, 1993, 657-667.

5. B. G. Thomas: "Mathematical Modeling of the Continuous Slab Casting Mold, a State of the Art Review", in *Mold Operation for Quality and Productivity*, A. Cramb, eds., Warrendale, PA, Iron and Steel Society, 1991, 69-82.

6. R. Bommaraju and E. Saad: "Mathematical modelling of lubrication capacity of mold fluxes", in *Steelmaking Proceedings*, **73,** Iron and Steel Society, Warrendale, PA, 1990, 281-296.

7. B. Ho: "Characterization of Interfacial Heat Transfer in the Continuous Slab Casting Process", Masters Thesis, University of Illinois at Urbana-Champaign, 1992.

8. B. G. Thomas, B. Ho and G. Li: *CON1D User"s Manual*, University of Illinois, , 1994.

9. C. A. Sleicher and M. W. Rouse: *Int. J. Heat Mass Transfer,* 1975, **18**, 677-683.

10. D. Larson: "Criteria for selecting mold powders to optimize continuous cast steel quality", *Industrial Heating,* 1986, **53**, 16-19.

11. M. C. Flemings: *Solidification Processing*, McGraw Hill, 1974, 17-19.

12. G. D. Lawson, S. C. Sander, W. H. Emling, A. Moitra and B. G. Thomas: "Prevention of Shell Thinning Breakouts Associated with Widening Width Changes", in *Steelmaking Conference Proceedings*, **77,** Iron and Steel Society, Warrendale, PA, 1994, 329-336.